CHAPTER 3
Effect of dopants on arsenene and zirconium chalcogenides based 2D catalysts towards hydrogen evolution reaction

3.1 Introduction

The energy demand is increasing exponentially day by day with the increase in world's population. However, the fulfilment of major energy demand depends on the fossil fuel which is not only limited but also causes major environmental issues, such as global warming, pollution etc. due to CO_2 emission.[1] To meet the world's clean energy demand, there is an urge to replace the non-renewable energy resources with renewable energy resources. However, the contribution of green energy production such as solar power, wind power, hydro-power and nuclear power over non-renewable energy is significantly less due to their strong dependence on environmental and geographical conditions.[2] The production of hydrogen is one of the best ways for having the clean energy to fulfil this energy demand gap.[3] Most of the techniques for the production of hydrogen again depends on the fossil fuels that does not resolve the major problem of CO_2 emission.[4] Electrochemical water splitting method is a simple method for the production of hydrogen from disassociation of water molecule.[5] This method has attracted both researchers and scientists as the required reactant water is abundantly available on earth and does not emit CO_2 as bi-product.[6–11] This method consists of two half reactions: one is hydrogen evolution reaction (reduction half reaction: $2H^+ + 2e^- \rightarrow H_2$; HER) which follows Volmer and Tafel reactions and other one is oxygen evolution reaction (oxidation half reaction: $2H_2O \rightarrow 4H^+ + 4e^- + O_2$; OER) that produces hydrogen and oxygen gas respectively by electrical bias or solar power.[7,12] This splitting process seems to be tough as it requires high activation energy to break the bond between O and H of water molecule. For this, we require a highly reactive catalyst which promotes and speed up the HER and OER activities.[13]

Till date platinum is considered as the best catalyst for HER; however, its low abundance and cost are major issues for having economical amount of hydrogen for overcoming the energy demand.[14,15] There is a need of an economic catalyst which should possess properties like large relative surface to volume ratio, high stability, low toxicity, abundant quantity and low cost. The catalysts are classified on the basis of source, that is, the catalysts whose source carrier is electrical bias in electrochemical cell are referred as electro-catalysts, and another one which utilizes the solar energy are referred as photo-catalysts. The electro-catalysts exhibit metallic or low band gap semi-conducting nature whereas the photo-catalysts mostly possess semi-conducting nature with band gap between 1-2 eV.[5,7] Many promising catalysts showing HER activity have been discovered such as nickel (Ni) alloys, platinum (Pt) and platinum alloys with other noble metals.[16–18] These catalysts also owe few drawbacks; such as the nickel alloy degrades in acidic medium, which can be overcome by utilizing Pt alloy, but they are expensive and less abundant.[16,19,20]

Two-dimensional (2D) materials owe the central place among diverse catalysts due to their unique properties particularly being them a promising HER catalyst. Extensive studies have been carried out in search of economical catalysts such as non-noble transition metals, carbides, transition metal phosphides and nitrogen or boron doped graphene, borophene, MoS_2, MoWS, VS_2,, VSe_2, WS_2, PtS_2, Mo_2C etc. for good HER and OER activities.[21–29] The adsorption of hydrogen and oxygen usually takes place on the surface of the catalyst; hence, it is expected that the surface of the two-dimensional materials might play a vital role in catalytic activity. Transition metal di-chalcogenides (TMDs) are perhaps the best surface dependent catalytic materials. These materials exhibit buckling geometry, unlike the planar structure of graphene and h-BN. Edge sites of TMDs are more active compared to the basal plane which is the major hindrance for the production of hydrogen. Besides this, together with the morphology and dimensionality of the catalysts, their electronic properties play an important role in the selection of a material to be utilized as a catalyst, as they can be served as electro or photo-catalyst. It was observed that the MoS_2 shows better catalytic activity at metallic zig-zag edge than its semi-conducting counter-part. The electronic properties of these 2D materials can be tuned by several approaches such as by chemical doping, creating defect and applying strain or electric field or pressure.[13,21,24,29]

The doping of heteroatoms which tunes the electronic properties by confining the electronic carriers reduces the recombination rate of photo-induced electrons/holes and creates structural defects responsible for the lifespan enhancement.[30,31] The enhancement of catalytic activity of the catalyst purely depends on the type of the dopant and its concentration. The catalytic activity of several 2D materials such as graphene with dopants B and N, VS_2 with dopants W and Ni, borophene with dopants C, N, P, S and Li etc. enhances.[21,25,30] Similarly, limitations in the case of TMD catalysts can be overcome with chemical doping and by creating defect responsible for the increased basal plane activity compared to their edge site activity.[13,23,29] Furthermore, most of the selenide based TMD catalysts show better catalytic activity than sulphur based TMD catalysts.[10] Recently, MoSSe Janus has been successfully synthesized and shown to have a better catalytic activity for HER compared to other TMDs (.i.e. SeMoS > SMoSe > $MoSe_2$ > MoS_2).[32–34] In addition, TMDs such as $ZrSe_2$ and $ZrTe_2$ have shown better catalytic activity that is comparable to the Pt based catalysts at low vacancy density, as their hydrogen adsorption free energy (ΔG) is found very close to zero whereas, ZrS_2 is shown to be highly efficient photo-catalyst.[35] Above studies motivate us to explore these 2D materials as catalysts for HER and OER activities beyond expensive Pt based catalysts.

In the present study, we have employed the first-principles calculations based on density functional theory with inclusion of dispersion correction to investigate the hydrogen evolution reaction (HER) and oxygen evolution reaction (OER) of pristine and doped arsenene and HER of pristine and doped ZrS_2, ZrSSe and $ZrSe_2$ monolayers. Of the particular interest, our major aim is to tune the electronic properties of these systems by chemically doping different atoms such as B, N, O, Ga, Ge and Se atoms for arsenene and Nb, Pt and W atoms for ZrS_2, ZrSSe and $ZrSe_2$. We have analyzed the role of dopants towards the enhancement of catalytic activity of these systems. To depict the reactivity of these systems towards hydrogen and oxygen and understand its role in catalysis, we have calculated the work-function of these systems.

3.2 Computational methods

All calculations were carried out using plane wave pseudopotential approach within the generalized gradient approximation (GGA)[36,37] as an exchange correlation functional implemented in Quantum espresso code.[38] In addition the depression correction is included throughout the calculations to avoid the non-accurate adsorption energy of the adsorbent and overcome the limitation of standard DFT which does not incorporate the long range dispersive forces.[39] The vacuum of 15 Å in the Z-direction has been introduced to neglect the interaction between two periodic units. In the case of pristine and doped arsenene, we used ultrasoft pseudopotentials to describe the atomic cores and valence electrons with an energy cutoff of 80 Ry and the charge density cutoff of 800 Ry for electronic wave function, whereas for pristine and doped ZrX ($X=S_2$, SSe and S_2), we used norm conversing pseudo potentials with the converged magnitudes of kinetic energy cut-off of 120 Ry. To achieve a good convergence, we have used an energy convergence threshold of 10^{-4} eV and maximum Hellmann-Feynman force acting on each atom was set to be less than 0.001 eV/Å. These parameters were sufficient to fully converge the lattice parameters and total energy of the considered systems. The reciprocal space was sampled by a dense grid with 9 x 9 x 1 and 8 x 8 x 1 **k**-points for arsenene and ZrX systems respectively. The Brillouin zone (BZ) integration was performed using Monkhorst-Pack convergence analysis.[41] In addition, for arsenene we have performed the spin-polarization calculation. Sabateir principle which is characterized by free energy of adsorption of reactive intermediate on surface is employed to investigate the HER and OER performances of the catalysts.[41] The HER and OER catalytic efficiency of given surface at equilibrium conditions can be determined by exchange current density that can be attributed to Gibbs free energy (ΔG).[21,42] The Gibbs free energy is expressed as follows:

$$\Delta G = E_{ads} + \Delta E_{ZPE} - T\Delta S \tag{3.1}$$

where, E_{ads} is the adsorption energy and ΔE_{ZPE} is the zero point energy difference of hydrogen and oxygen atoms in the adsorbed phase and gas phase which ranges from 0.01 to 0.04 eV for hydrogen [21,43] while for oxygen it is close to zero.[44] ΔS is the entropy of H and O, which is of the order of 0.24 and 0.33 eV respectively. The adsorption energy for hydrogen and oxygen after simplification leads to $\Delta G_H = E_{ads} + 0.24$ and $\Delta G_O = E_{ads} + 0.33$ respectively. The hydrogen and oxygen chemisorption energies are defined as:

$$E_{ads\ H} = E_{(System+H)} - E_{(SYstem)} - \frac{1}{2}E(H_2) \tag{3.2}$$

$$E_{ads\ O} = E_{(System+O)} - E_{(System)} - \frac{1}{2}E(O_2) \tag{3.3}$$

where, $E_{(system+H)}$, $E_{(system+O)}$, $E_{(system)}$, $E(H_2)$ and $E(O_2)$ are the total energies of hydrogen adsorbed nanosheet, oxygen adsorbed nanosheet, nanosheet without adsorption, isolated hydrogen molecule and isolated oxygen molecule respectively. The change in the work-function is an important parameter for the determination of catalytic activity as it determines the presence of minute amount of contamination on a monolayer or occurrence of surface reaction. The higher value of the work-function of a catalyst suggests to have strong binding surface and more sensitivity towards the morphology. The energy difference between Fermi and electrostatic or potential vacuum level is basically considered as work-function of materials and is expressed as

$$\varphi = V_l - \mathrm{E_f} \tag{3.4}$$

where φ, V_l and $\mathrm{E_f}$ are work-function, vacuum level or electrostatic potential and Fermi energy respectively. The open circuit potential in aqueous electrolyte can be calculated using the following equation.[45]

$$V = \frac{\varphi}{e} - 4.44 \tag{3.5}$$

where, 4.44 V is the recommended value of absolute potential of the standard hydrogen electrode.[46]

3.3 Results and discussion

In this work, we systematically investigated the structural and electronic properties of pristine arsenene and monolayer of ZrS_2, ZrSSe and $ZrSe_2$ from catalytic point of view and for the enhancement of catalytic activity of these systems we sieved these systems with different dopants.

3.3.1 Arsenene with B, N, O, Ga, Ge and Se dopants

The study of the geometrical structure and electronic properties of catalyst is important for the proper choice of a good catalyst. Furthermore, catalytic activity of a catalyst depends on its stability and interaction between adsorbate and adsorbent for which the structural properties of a catalyst is important. The optimized structure of monolayer arsenene is shown in Fig. 3.1(a). This figure also depicts the optimal buckled height, bond length and lattice constant of monolayer arsenene which are 1.389 Å, 2.503 Å and 7.1679 Å respectively. The calculated electronic band structure of pristine arsenene is shown in Fig. 3.1(b). The arsenene exhibits semi-conducting nature with indirect band gap of 1.62 eV consistent with the previous work.[48] The most important descriptors for the photocatalytic activity are the band gap and recombination possibility of electrons and holes which make band analysis an important factor to understand the catalytic mechanism for catalysts. Fig. 3.1(b) clearly depicts significant dispersive nature of

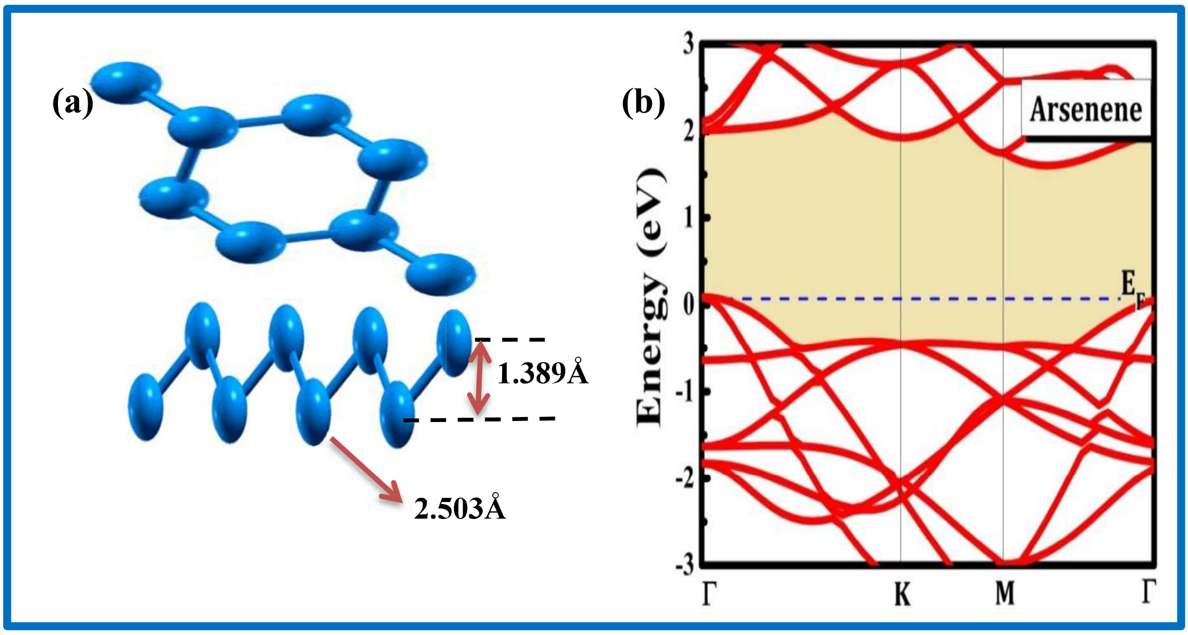

Figure 3.1: (a) Top and side view of optimized geometric structure of buckled arsenene (b) electronic bands structure of arsenene using PBE exchange-correlation function.

bands near top of the valence band region at **Γ-**point of the BZ indicating low hole effective mass. This suggests arsenene to be a good photocatalyst for HER and OER.[21]

Table 3.1: The optimized lattice constant, bandgap, work-function and adsorption energy of hydrogen and oxygen with pristine and functionalized arsenene.

System	Lattice constant (Å)	Bond length (Å)	Band gap (eV)	Work-function ϕ(eV)	ΔE_H (eV)	ΔE_O (eV)
Arsenene (As)	**7.1679**	**2.50**	**1.62**	**1.83**	**-1.27**	**-2.85**
As-B	**7.071**	**2.06**	**0.74**	**1.75**	**-2.00**	**-0.37**
As- N	**6.857**	**2.02**	**0.65**	**1.59**	**-2.90**	**-3.93**
As- O	**6.947**	**2.12**	**-**	**1.44**	**-0.24**	**-4.021**
As- Ga	**7.339**	**2.40**	**1.7**	**1.48**	**-1.50**	**-4.87**
As- Ge	**7.346**	**2.46**	**0.57**	**1.34**	**-2.04**	**-3.53**
As- Se	**7.289**	**2.59**	**-**	**0.78**	**-1.59**	**-0.04**

Next, we adsorbed the hydrogen and oxygen atoms on arsenene nano sheet to know its capability towards its catalytic activity. The adsorption energy of hydrogen and oxygen over arsenene at edge sites is -1.27 eV and -2.85 eV respectively (see Table 3.1). The optimal adsorption energy for hydrogen is 0.24 eV, that leads to the Gibbs free energy Zero ($\Delta G = 0$) to be a good catalyst. In the process of reactions, initially molecules collide simultaneously in gas phase outwit to surface of arsenene and the occurrence of reaction depends on the interaction between molecule and adsorbate. To adsorb adsorbate to the surface of catalyst, the catalyst should react strongly to the reagent and intermediates. However, catalyst should not bind too strong to intermediate or product that might make the desorption of the product difficult.

In nutshell as per the Sabatier principle, optimal catalyst should bind strong enough to the reagents for reaction to happen and weakly to product so that they would desorb easily. The adsorption energy of pristine arsenene shows its better chance for HER performance. The dopants enhance the catalytic activity of materials by altering its fundamental bandgap, therefore we now turn our attention towards the functionalization of arsenene.[47,48] We have functionalized the pristine arsenene with B, N, O, Ga, Ge and Se dopants.

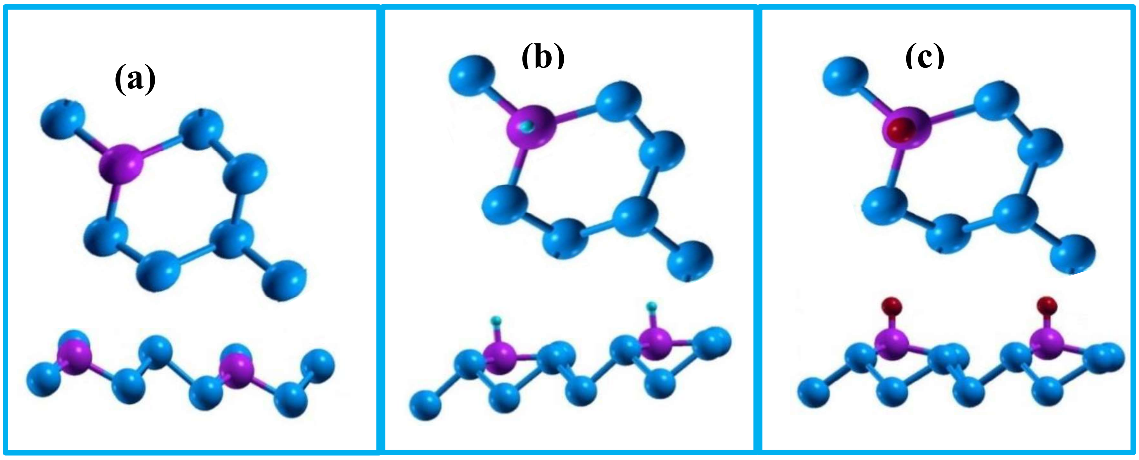

Figure 3.2:(a) Top and side view of functionalized arsenene, purple sphere as dopants (B, N, O, Ga, Ge and Se) and sky-blue sphere one As. (b) Cyan sphere is hydrogen adsorbed on dopant atoms. (c) Red one sphere is oxygen adsorbed on dopant atoms

We have substituted one As atom in the supercell by one B, N, O, Ga, Ge and Se atoms leading to 12.5 % of impurity concentration. Fig. 3.2(a) presents the optimized structure of B, N, O, Ga, Ge and Se atoms functionalized arsenene. The As-B, As-N and As-O bond lengths decrease due to the small atomic radii and strong electro negativity of B, N, O dopants. However, on the other hand, the bond length between As and Ga, As and Ge and As and Se differs lesser compared to As-As bond length (see Table 3.1) from their lesser structural distortion arising from the almost same atomic radii and electronegativity. We observe that the accumulation of electrons at Fermi level differs with nature that is their electronegativity and

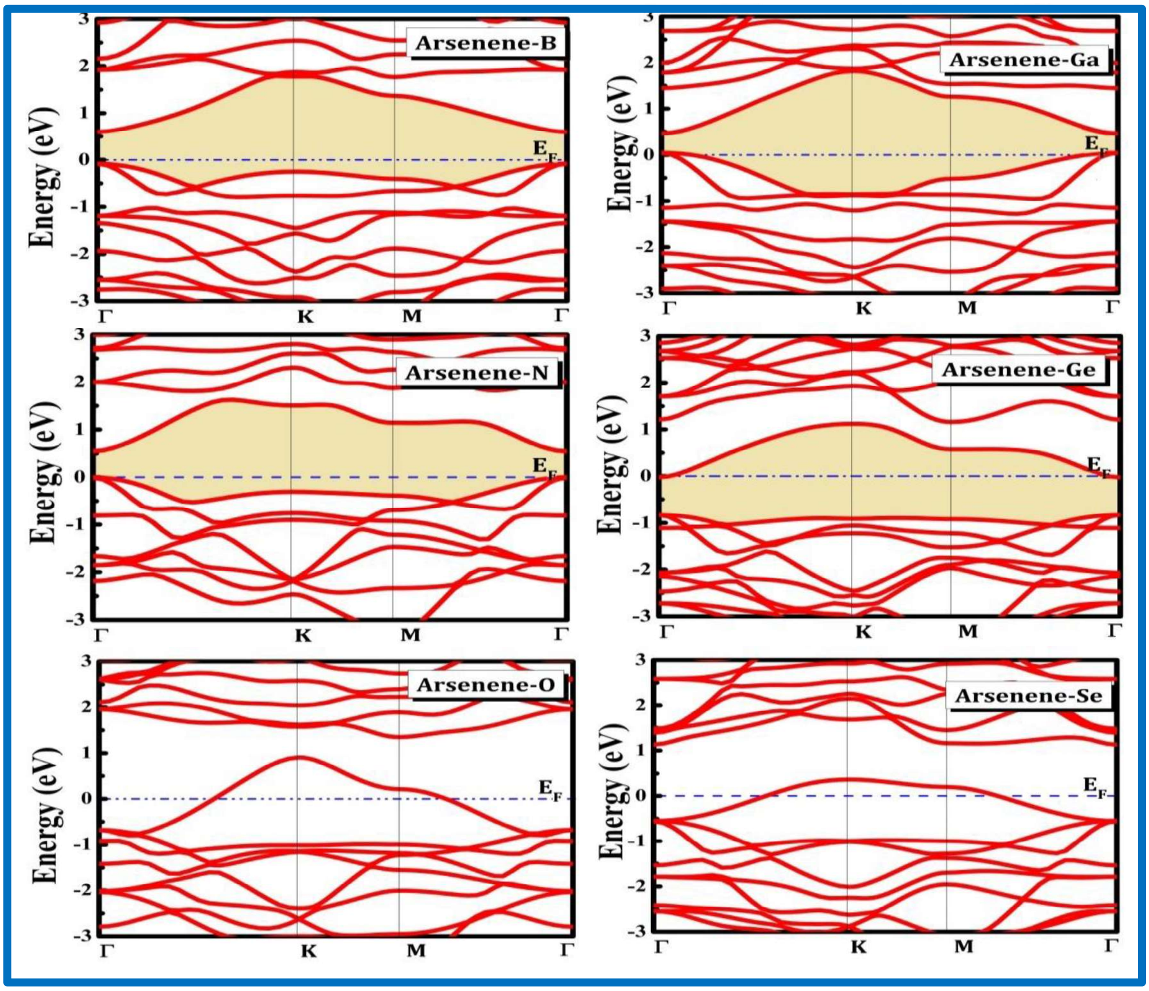

Figure 3.3: The band structure of the B, N, O (left panel) and Ga, Ge and Se (right panel) doped arsenene.

valences of dopants. This can be seen from the band structure of functionalised arsenene (see Fig. 3.3); that the B, N and Ga functionalized arsenene show p-type nature as Fermi level is close to maximum of valence band with band gap of 0.74, 0.65 and 1.7 eV respectively while Ge doping results into the n-type nature as Fermi level is close to minimum of conduction band with 0.57 eV band gap. The fundamental band gap of arsenene decreases with B, N and Ge doping whereas it increases with Ga doping. This can be attributed to the decreasing contribution of electrons from 's' orbit of B, N and Ge to conduction band, while in case of Ga functionalized arsenene, 'd' orbit contribution increases to valence band. All dopant show direct band gap nature at **Γ**-point except O and Se functionalised arsenene which show the metallic nature.

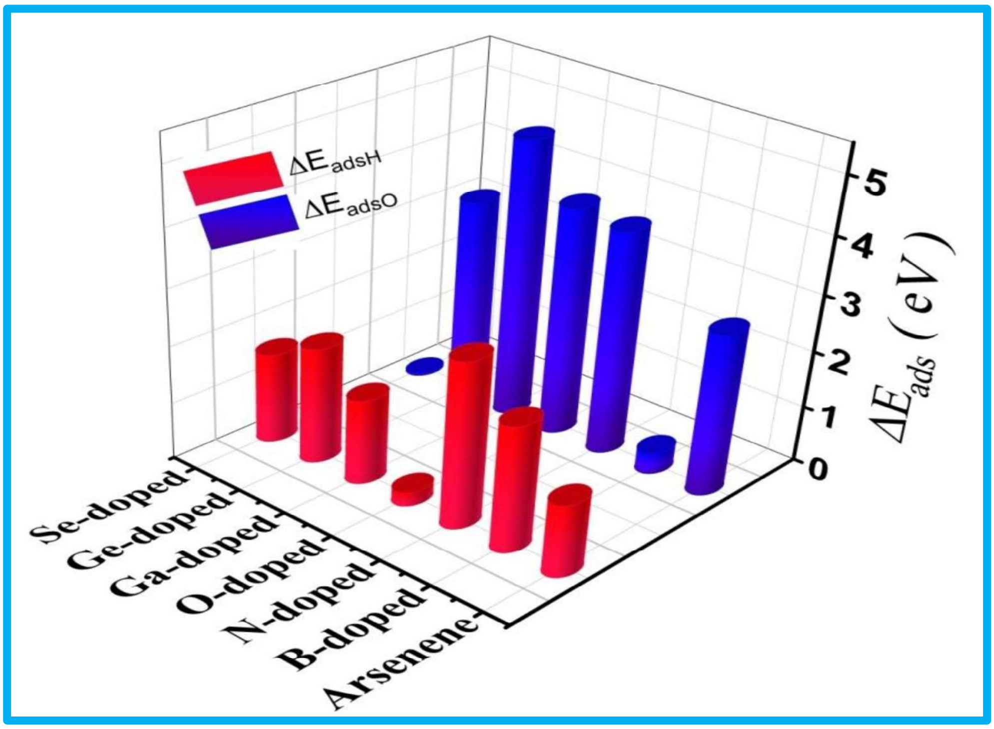

Figure 3.4: The adsorption energy of hydrogen and oxygen on pristine and B, N, O, Ga, Ge and Se doped arsenene.

We have calculated the hydrogen adsorption energy of functionalized arsenene using equation (3.2) which depicts that the adsorption energy of hydrogen increases with other dopants except O as shown in Fig. 3.4. For OER, the adsorption energy increases with O, Ga and Ge while it decreases with B, N and Se dopants. We observe that among all dopants, the functionalization of arsenene with B and Se dopants shows different trend. Further, we found that the electronegativity comes into picture for adsorption process of H and O as functionalization with B offers better OER catalytic effect whereas Se offers less affection towards O due to same electronegativity.

We have also calculated the work-function to authenticate the catalytic activity of pristine and functionalized arsenene. We notice that the work-function gradually decreases from As to O and increases for Ga and again decreases gradually for Se (Table 3.1). The O and Se doping show a different nature compared to other dopants. To understand these changes, we need a deeper understanding in terms of chemical properties of dopants. The dopants B, N, Ga and Ge have three valence electrons in outer most orbit, which are satisfied by nearest As atoms and this saturated bond makes pristine arsenene semi-conducting. The O and Se have +2 oxidation state at stable configuration which induces one non-bonding electron leading to unfilled highest valence band and defect band localised at Fermi level (Fig. 3.3). The O and Se contribute only two valence electrons to nearest As atoms that form bond. The one defect bond leads to metallic nature. Moreover, O shows good HER catalytic effect as its adsorption energy is -0.24, while, this is not the case with Se atom due to the difference in valence electron and electronegativity. Since Se atom can have more valence electrons in excited state and is less electronegativity as compared to oxygen, it results into strong adsorption energy with hydrogen atom. Similar trend is observed in the case of B and N atoms as both contribute same number of valence electrons to arsenene nano sheet. The N atom is more electronegative compared to B atom which makes B atom binding weaker with oxygen compared to nitrogen and other dopants.

The density of states for H-adsorbed and O-adsorbed arsenene and functionalised arsenene sheet provide deeper insight and justification for the binding of hydrogen and oxygen with arsenene and dopants through the contribution of H and O near Fermi level. Fig. 3.5(a) presents the density of states (DOS) of isolated hydrogen atom, H adsorbed arsenene, and functionalized arsenene. From the contributions of different levels in the DOS near Fermi level, the quality analysis of adsorption energy and bonds is possible.[49] The strength of the bond is determined by the contribution of the adsorbent valence electron and changes in the adsorbent DOS. More contribution of valence electrons to adsorbent leads to the electron distribution in adsorbent bonding and anti-bonding states, which tends to disappear near Fermi level. In addition, less contribution of PDOS of adsorbate towards adsorbents is due to physisorption. In the case of O doping, there is a presence of DOS due to hydrogen, which means a less contribution to the anti-bonding states, that is consistent with our adsorption energy results. The other dopants show strong binding towards hydrogen as hydrogen contributes more to bonding and anti-bonding states. Similar trend in bonding is observed in case of oxygen adsorption over B doped arsenene as shown in Fig. 3.5(b). The PDOS of oxygen contributes less to anti-bonding states resulting in weak interaction with B doped arsenene in contrast to other which show strong binding. All results are consistent with the calculation of oxygen adsorption energy. The present

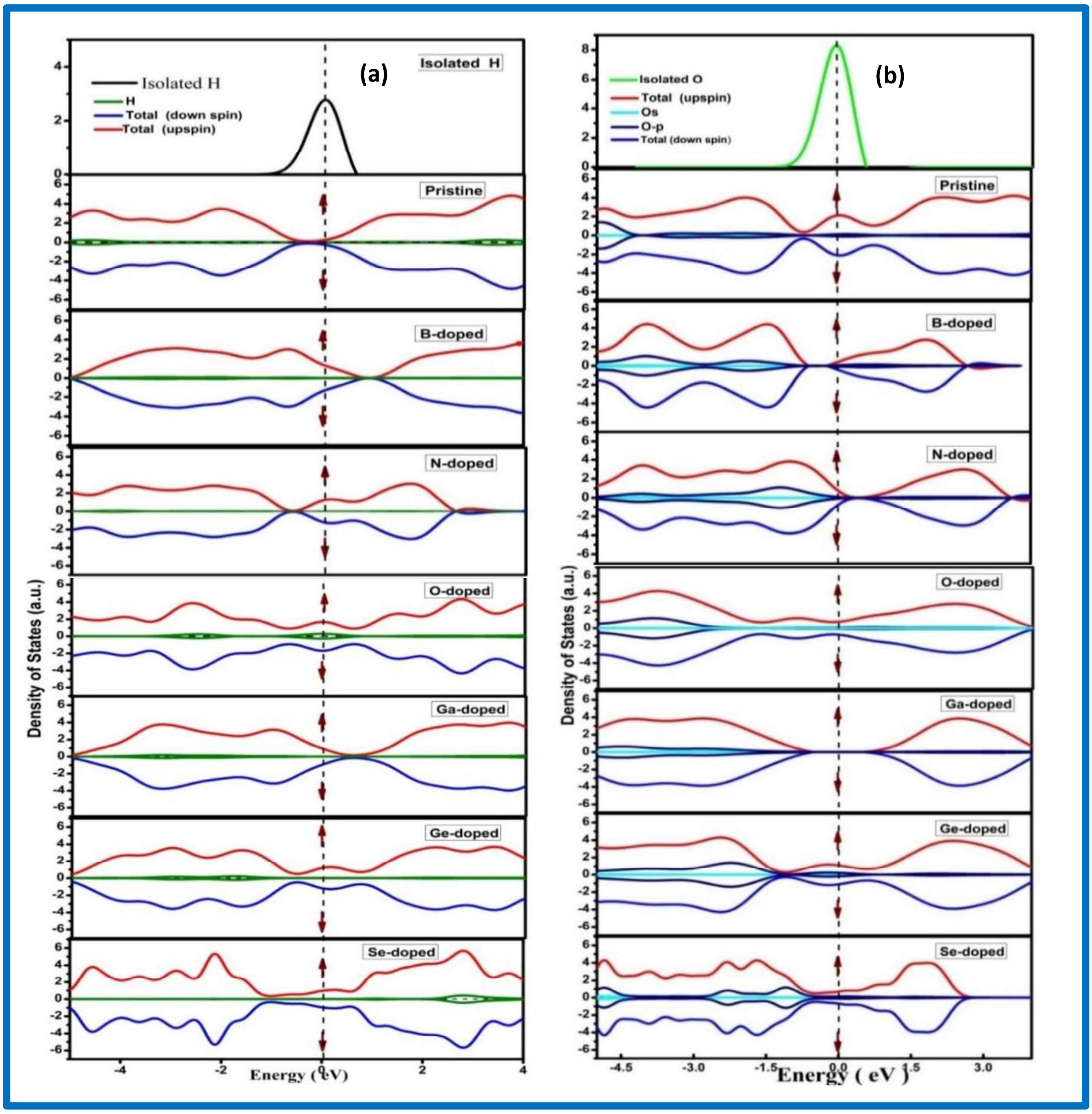

Figure 3.5: (a) shows the density of states of isolated H and H adsorbed on pristine arsenene and doped arsenene and (b) the density of states of isolated O and O adsorbed on pristine and doped arsenene.

calculation on pristine and Ga, Ge and Se doped arsenene shows a strong binding of hydrogen and oxygen atoms indicating desorption process difficult. The most promising candidate for HER is O doped arsenene as its adsorption energy is -0.24 eV, whereas B doped arsenene is the most promising candidate for OER among all considered dopants as it has adsorption energy of -0.37 eV very close to required -0.33 eV.

3.3.2 ZrS$_2$, ZrSe$_2$ and Janus ZrSSe with Nb, Pt and W dopants

Before performing a detail calculation, we optimized individual the ground state stable T-phase of ZrX$_2$ (X=S, Se). The corresponding space group for ZrX$_2$ is $P\bar{3}m1$ (No. 146). Zirconium (Zr) is coordinated by six chalcogen atoms forming an octahedral symmetry (O$_h$ symmetry) as presented in Fig. 3.6(a-c). Janus ZrSSe is TMD monolayer of ZrX$_2$ (X=S, Se) where one of the chalcogen layer i.e. Se is replaced by a layer of other chalcogen atom i.e. S layer or vice-versa.

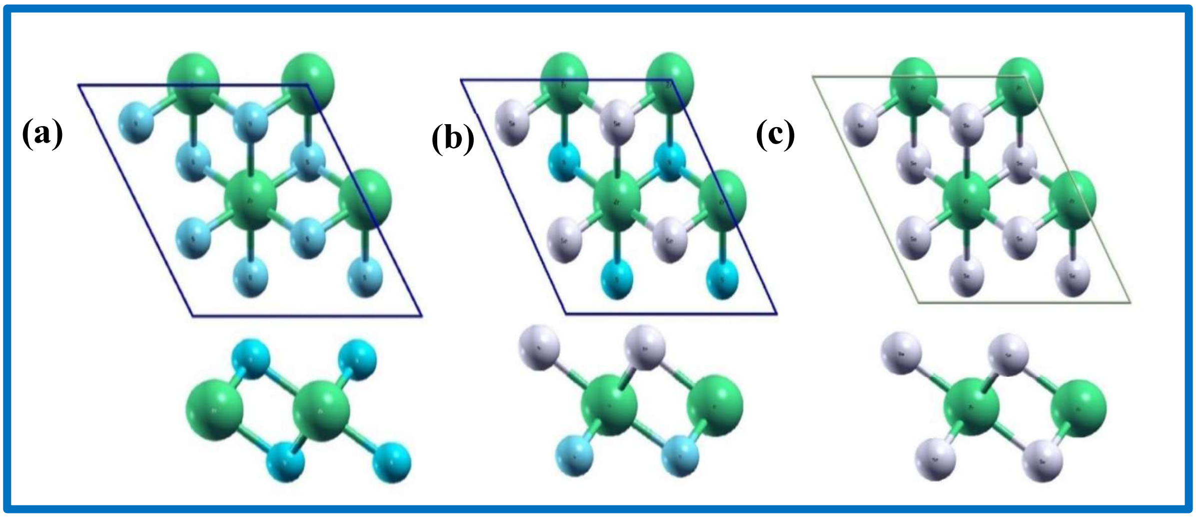

Figure 3.6: The optimized geometries of pristine (a) ZrS$_2$, (b) ZrSSe and (C) ZrSe$_2$. Box in the top represents the unit cell considered for the calculations.

In addition, due to the replacement of one of the layers, a distortion of the out-of-plane symmetry is observed that reduces the symmetry of Janus. The ground state of Janus is also 1T phase. However, it has low symmetric space group P3m1 (No. 156). Table 3.2 shows that the bond lengths Zr-S and Zr-Se for Janus ZrSSe are 2.59 Å and Janus 2.72 Å respectively. The optimized lattice constant of the unit cell of ZrS_2, ZrSSe and $ZrSe_2$ is 3.66 Å, 3.76 Å and 3.82 Å respectively, which is in good agreement with pervious data.[50,51] The Fig. 3.7(a-c) presents the band structure of 2x2 supercell of ZrS_2, Janus ZrSSe and $ZrSe_2$ monolayers. The band gap of ZrS_2, Janus ZrSSe and $ZrSe_2$ is 1.58 eV, 1.08 eV and 0.84 eV respectively, which is consistent

Table 3.2: Calculated band gap (Eg), bond length, work-function, hydrogen adsorption and Gibbs free energy for pristine systems.

Pristine	Lattice constants (Å)	Band gap (eV)	Bond length (Å)	Work-function φ (eV)	ΔE_H (eV)	ΔG_H (eV)
ZrS_2	7.311	1.58	2.591	6.44	1.57 (Basal plane)	1.81
					0.98 (Edge Site)	1.22
ZrSSe	7.524	1.08	2.59 (Zr-S) 2.719 (Zr-Se)	5.87	1.43 (Basal plane)	1.67
					0.95 (S-Edge)	1.19
					1.31 (Se-Edge)	1.55
$ZrSe_2$	7.641	0.85	2.718	5.47	1.65 (Basal Plane)	1.89
					1.1 (Edge Site)	1.34

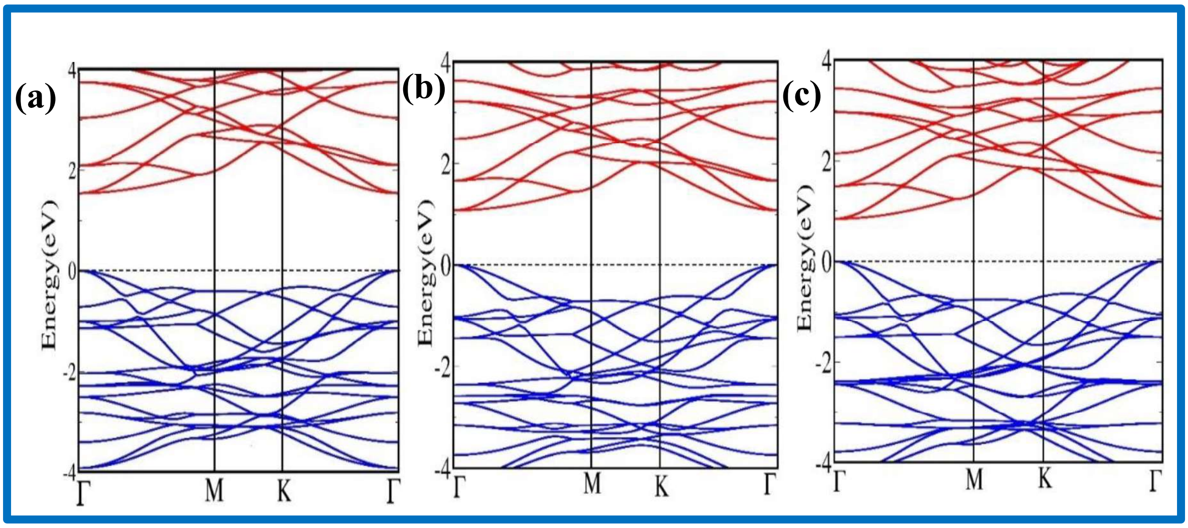

Figure 3.7: The calculated band gap of pristine (a) ZrS_2, (b) ZrSSe and (C) $ZrSe_2$. Red and blue curves represent conduction and valence bands respectively.

with the reported data.[51] The Janus monolayer exhibits band gap in between the ZrS_2 and $ZrSe_2$ due to the incorporation of Se atoms in place of S atoms with reference to counterpart ZrS_2, that leads to the reduction in band gap as compared to pristine ZrS_2. The band gap of both ZrS_2 and ZrSSe lies within the range of 1-2 eV suggesting them to be potential photo-catalysts while, $ZrSe_2$ can be used as an electro-catalyst as it exhibits low band gap. In general, Janus TMDs have been shown better catalysts for HER as compared to their counterpart TMDs due to their asymmetric nature.[10] Moreover, for having good catalytic activity, the catalyst must have an optimal (Zero) Gibbs free energy. Besides, if Gibbs free energy is found too negative, hydrogen will bind strongly to the surface of the catalyst making it difficult to desorb. On the other hand, if Gibbs free energy is too positive, it will result in weak binding of hydrogen to the catalyst, which will cause problem with adsorption.[7] The optimal Gibbs free energy and hydrogen adsorption energy for HER is 0 and -0.24 eV, respectively (as described in computational section).

TMDs show good catalytic activity in the vicinity of edge sites rather than basal planes.[21] We therefore studied the hydrogen adsorption at various sites on the edges and the basal planes. There are two edge sites for Janus: the sulfur site referred as the S-edge site and the selenide site referred as the Se-edge site. We used equations 3.1 and 3.2 to calculate both hydrogen adsorption and Gibbs free energies for ZrS_2 on the edges and basal plane. The ZrS_2 shows good catalytic activity on the edge site rather than on the basal plane and the difference in Gibbs free energy is about 48%. Similar trends have been observed for $ZrSe_2$ where its edge is 29 % more active than its basal plane. The present trends are in the good agreement with the previous studies on $ZrSe_2$.[13] The calculated Gibbs free energy of the previously reported ZrS_2 is 16 % lower than that of $ZrSe_2$, whereas we found only about 4 % lower with the inclusion of dispersion correction. In addition, the comparison between ZrS_2 and $ZrSe_2$ reveals that the sulfur edge is more active than the selenide edge; whereas for TMDs in general, the selenide catalyst is found more active than the sulfur counterpart.[10] The Gibbs free energy of Janus is very close to zero due to occurrence of edge adsorption rather than basal plane. It is interesting to note an increase in catalytic activity on the edge side due to high asymmetric arrangement of the atoms in Janus. The Janus also shows that the edge of the sulfur is more active than the edge of selenide.

Lastly, we compare Gibbs free energy calculated at basal plane and edge site for all three systems, and observe following sequence for HER activity, SZrSe > SeZrS > ZrS_2 > $ZrSe_2$ with

SZrSe being best among remaining counterparts; where SZrSe refers to the hydrogen adoption at S edge-site and SeZrS to the Se-edge-site. The Janus ZrSSe shows good catalytic activity for HER compared to counterpart TMDs. This is similar to the trend as observed in Janus SeMoS.[33] The higher catalytic activity of ZrS_2 compared to $ZrSe_2$ can be attributed to the higher Pauli electronegativity of S (2.58 eV) than Se (2.55 eV). The electronegativity of Zr (1.33 eV) is least after Hafnium (1.3 eV) among all transition metal elements which show different trends of charge transfer towards hydrogen atom compared to other TMDs. We have calculated Lowdin charge to understand the charge transfer and the interaction between the catalyst and the hydrogen atom. We observe that the charge is transferred to the hydrogen atoms from the catalyst. The electron accumulations reflect the relative electronegativity difference for ZrS_2, Janus ZrSSe and $ZrSe_2$. We found that the relative electronegativity of Se and S is quite low and the charge transfer at the edge site for ZrS_2 and $ZrSe_2$ is 0.19e and 0.5e respectively. However, in case of Janus, for both edges S and Se, charge transfer is about 0.19e and 0.25e respectively. It is difficult to conclude on the reactivity of ZrS_2 and Janus ZrSSe at the sulfur edge-site due to their small electronegativity difference. However, we can certainly conclude that the $ZrSe_2$ binds strongly to the edge-site hydrogen leading to chemisorption. Similar trends are observed in basal planes where charge accumulation in hydrogen atoms for ZrS_2, ZrSSe and $ZrSe_2$ is about 0.27e, 0.23e and 0.3e respectively. The adsorption of hydrogen is in the following sequence ZrSSe > ZrS_2 > $ZrSe_2$ which is consistent with the above-mentioned Gibbs free energy calculations.

We also calculated the work-function of ZrS_2, $ZrSe_2$ and Janus ZrSSe to confirm our results more accurately. Work-function can be related to HER's interface descriptor as it is an analogy to describe the capability of the catalyst to adsorb hydrogen.[45] The optimal work-function of the most efficient Pd and Pt catalysts for HER is 5.12 eV and 5.56 eV respectively.[52] The work-function determines M-H bond strength, where M is metal transition. In most of the cases, higher magnitude of work-function leads to higher positive adsorption energy towards hydrogen.[45] The ZrS_2 exhibits higher work-function than $ZrSe_2$ resulting in higher positive ΔE_H for ZrS_2 than $ZrSe_2$. The calculated open circuit potential is 2 V, 1.43 V and 1.03 V respectively for ZrS_2, ZrSSe and $ZrSe_2$. We calculated partial electronic density of states (PDOS) for

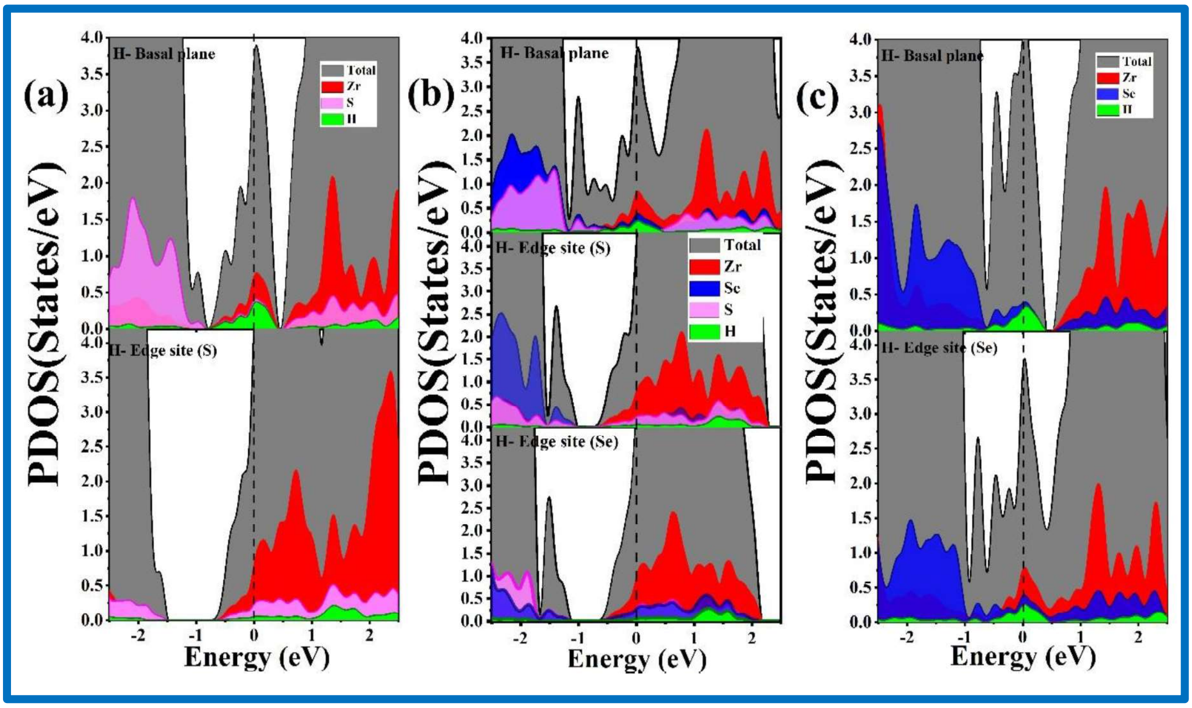

Figure 3.8: The calculated PDOS of hydrogen adsorbed at basal plane and edge-site of (a) ZrS_2, (b) ZrSSe and (C) $ZrSe_2$.

hydrogen adsorbed ZrS_2, Janus ZrSSe and $ZrSe_2$ at basal plane and edge-site to gain deeper insight into hydrogen adsorption at various locations. The ZrS_2, Janus ZrSSe and $ZrSe_2$ show metallic nature after adsorption of hydrogen (see Fig. 3.8(a-c)) that confirms the interaction between hydrogen and catalyst. The formation of the bond between the hydrogen atom and the adsorbent can be confirmed with presence of hydrogen PDOS near Fermi level. We also observed that the for hydrogen is denser near Fermi level for the ZrS_2 basal plane, which can be attributed to the nature of chemisorption that is consistent with the results of Gibbs free energy. Similar nature is observed in PDOS of ZrSSe and $ZrSe_2$ for basal plane adsorption. The weaker interaction between hydrogen and adsorbate gives rise to bonding and anti-bonding states that leads to easy desorption of hydrogen. The PDOS also confirms that the edge-site of ZrS_2 and ZrSSe is more active compared to basal plane. The ZrSSe is better catalyst than ZrS_2 and $ZrSe_2$ despite quite active edge site of ZrSSe. Previously, the active edge-site of TMD catalysts was claimed as one of the barriers to hydrogen production,[10,53,54] which suggests of a need to increase the activeness of basal plane. The activity of TMD basal plane after doping with different dopants increases.[55,56] This suggests an improved catalytic activity of ZrS_2, ZrSSe and $ZrSe_2$ after doping. To investigate the effect of doping on pristine ZrS_2, ZrSSe, and $ZrSe_2$ on HER performance, we replaced one of the supercell's Zr atoms with dopant Nb, Pt, and W as shown in the Figure 3.9(a-c). It is known that the tuning of fundamental electronic properties of host material enhances its catalytic activity. We have optimized all functionalized systems and found no substantial structural distortions. The lattice constant of the pristine ZrS_2 decreases with Nb

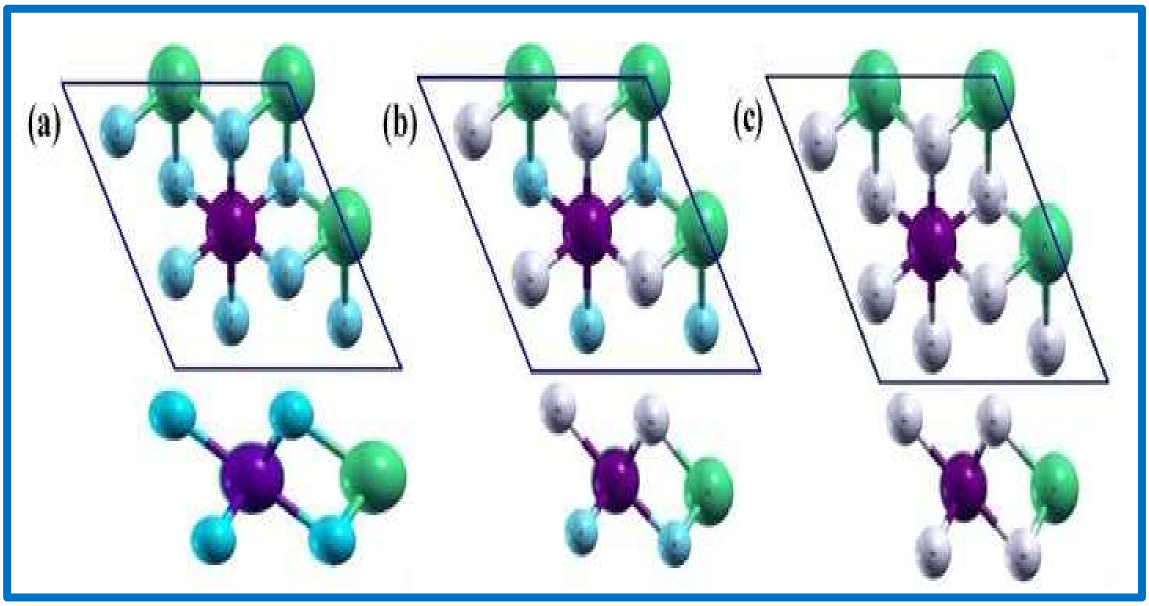

Figure 3.9: Top and side views of the optimised geometries of doped (a) ZrS_2, (b) ZrSSe and (C) $ZrSe_2$; purple sphere represents dopants (Nb, Pt and W), sky blue sphere represents S atoms, white atoms represents Se and Green sphere represents Zr atoms respectively. Box in the top represents the unit cell considered for the calculations

and Pt dopants while it increases with W, which can be attributed to the smaller ionic radius of dopants than Zr whereas ionic radius of W is bigger than Zr (see Table 3.3). This decrease can also be related to the compressive strain produced on the host structure due to doping. However, observed increment in the lattice constant with W dopant can be related to the tensile strain produced in the structure. A similar trend is observed with the lattice constant for Janus ZrSSe and $ZrSe_2$, where the lattice constant decreases with the W, Pt and Nb-dopant (Table 3.3). We notice that the lattice constant of functionalized systems depends on dopants and chalcogenides' relative electronegativity. The lattice constant of W-functionalized ZrS_2 increases compared to pristine, whereas for W functionalized ZrSSe and $ZrSe_2$ it decreases. Now, we turn our attention

Table 3.3. Calculated work-function, hydrogen adsorption and Gibbs free energy for doped systems.

Doped systems	Lattice constants (Å)	Work-function φ (eV)	ΔE_H (eV)	ΔG_H (eV)
Nb- ZrS_2	**7.245**	**5.22**	**0.57**	**0.91**
Pt -ZrS_2	**7.283**	**6.31**	**0.54**	**0.78**
W -ZrS_2	**7.370**	**6.37**	**1.06**	**1.3**
Nb -ZrSSe	**7.355**	**5.14**	**0.55**	**0.79**
Pt -ZrSSe	**7.403**	**5.87**	**1.42**	**1.66**
W-ZrSSe	**7.492**	**5.84**	**1.43**	**1.67**
Nb -$ZrSe_2$	**7.468**	**4.81**	**0.39**	**0.63**
Pt -$ZrSe_2$	**7.527**	**5.28**	**1.42**	**1.66**
W-ZrSe2	**7.623**	**5.44**	**1.59**	**1.83**

to the electronic band structure of functionalized ZrS_2, Janus ZrSSe and $ZrSe_2$. It can be seen from Fig. 3.10(a-c) that the Nb doped ZrS_2, Janus ZrSSe and $ZrSe_2$ have a robust metallic character due to significant DOS at Fermi level in contrast to the Pt and W-doped ZrS_2, Janus ZrSSe and $ZrSe_2$ where DOS at Fermi level is almost negligible. We adsorbed hydrogen on top of the dopants to check the enhancement of HER after functionalization of all systems. Using equation 3.1, we calculated hydrogen adsorption and Gibb's free energy of all functionalized systems. We analyzed each functionalized system's Gibbs' free energy one by one. We found that all three dopants increase the catalytic activity of basal planes compared to pristine-ZrS_2. In addition, the system's basal plane activity depends on the nature of the dopant, i.e. its electronegativity, oxidation states, and electronic contribution. The oxidation states for Pt and

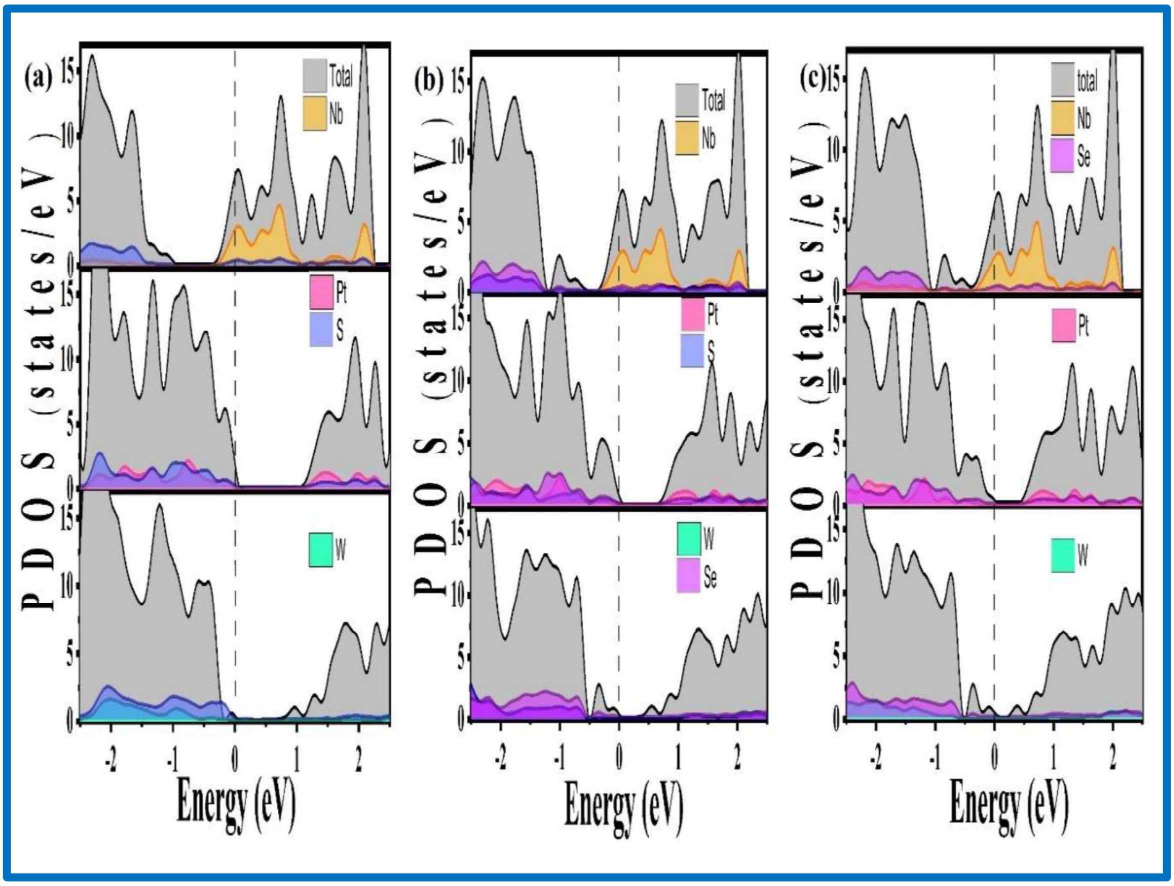

Figure 3.10: The calculated PDOS of functionalized (a) ZrS2, (b) ZrSSe and (C) ZrSe2 with dopant Nb, Pt and W respectively.

W varies from + 2 to + 6, whereas for Zr and Nb it varies from + 5 to + 4. All dopant's relative electronegativity is higher than Zr. The W-functionalized ZrS_2 has higher Gibbs free energy due to its high electronegativity whereas Pt-ZrS_2 has least Gibbs free energy. However, the Janus ZrSSe and Nb-ZrSSe have less Gibbs free energy. Similar trend is observed in the case of functionalized $ZrSe_2$. The Nb-$ZrSe_2$ has lowest Gibbs free energy among all considered systems. We conclude that the Nb-$ZrSe_2$ is best suited for HER as its value is closer to zero and follow the sequence for Gibbs free energy as Nb-$ZrSe_2$ > Pt-ZrS_2 >Nb-ZrSSe > Nb-ZrS_2 > ZrSSe. Using equation (3.5), we have calculated the open circuit potential for Nb-$ZrSe_2$, Pt-ZrS_2, Nb-ZrSSe, Nb-ZrS_2 and found 0.37 V, 1.87 V, 0.7 V and 0.78 V respectively. We found that the Nb-$ZrSe_2$ exhibits lowest open circuit potential and Pt-ZrS_2 exhibits highest open circuit potential which is also comparable to Pt. The lower open circuit potential value of Nb-$ZrSe_2$ indicates that it will dissolve faster and is less stable than Pt-ZrS_2.

Finally, we conclude that the functionalization helps in increasing TMD's basal plane activity. HER activity of catalysts depend not only on the Gibb's free energy but also on work-function and open circuit potential. The catalytic activity of Janus ZrSSe is better than its TMDs counterpart (ZrS_2 and $ZrSe_2$) and Nb-$ZrSe_2$ shows best catalytic activity for HER followed by Pt-ZrS_2, Nb-ZrSSe, Nb-ZrS_2 and ZrSSe.

3.4 Conclusions

In this study, we have investigated the structural and electronic properties of arsenene, ZrS_2, Janus ZrSSe. and $ZrSe_2$ monolayers under the framework of dispersion corrected density functional theory. We observed that all considered systems exhibit semiconducting nature with bandgap of 1.6 eV, 1.58 eV, 1.08 eV and 0.85 eV, respectively. The band gap of arsenene, Janus ZrSSe and ZrS_2 monolayers is suitable for their use as photocatalyst for water splitting process for the production of hydrogen, whereas the bandgap of $ZrSe_2$ monolayer is suitable for its use as an electro-catalyst. We have also analysed the surface chemistry of these monolayers to get a deep insight to the catalytic activity. From the adsorption energy calculations, we observe that the arsenene is well-suited for HER catalyst, rather than OER catalyst as arsenene binds oxygen strongly which is not suitable for a good catalyst. Thereafter, we tuned its electronic properties and surface reactivity by means of doping different dopants such as B, N, Ga and Ge to enhance the catalytic activity of arsenene for HER and OER. We observed that the arsenene after doping B, N, Ga and Ge preserves semi-conducting nature while O and Se-doped arsenene turn into metallic with defect bonding. The calculated work-function of these systems validate the results on adsorption energy and surface reaction characteristics. From adsorption energy and work-function calculations, we arrived at conclusion that among all considered arsenene systems, O doped arsenene shows better performance for HER activity followed by pristine and Ga doped arsenene. In case of OER, B doped arsenene performs better for catalytic activity followed by pristine and Ge doped arsenene. These results indicate that the dopants help to enhance the catalytic activity of the materials, as the metallic catalysts show better catalytic activity as compared to semi-conducting catalyst. We further investigated the zirconium chalcogenide monolayers for their applicability as an HER catalyst. We observe that the Janus ZrSSe monolayer is a better catalyst compared to ZrS_2 and $ZrSe_2$ monolayers at edge-site. Similarly, the edge-site of ZrS_2 and $ZrSe_2$ monolayers are found to be active for HER activity, whereas, the basal planes are inactive. We have doped all three systems with Nb, Pt and W atoms, and found that the Nb-doped systems have robust metallic nature and other systems possess usual metallic nature. We observe that the metallic systems show good catalytic activity compared to the semi-conducting catalysts, similar to the case of arsenene. On the basis of calculation of hydrogen adsorption and Gibbs free energy, we conclude that the Nb-$ZrSe_2$ is well suited for HER activity, followed by Pt-ZrS_2, Nb-ZrSSe, Nb-ZrS_2 and ZrSSe. The functionalization of these systems improves the basal catalytic activity of systems, as the Gibbs free energy of $ZrSe_2$ is positive among all three systems leading to desorption process feasible. This leads to poor adsorption of hydrogen on basal plane. After functionalization with Nb-dopant, the $ZrSe_2$ monolayer shows better catalytic activity among all the considered zirconium-based systems. In fact, the enhancement of HER activity of systems depends on selectivity of dopant material in both cases. Comparing two systems: arsenene and zirconium chalcogenide monolayers, we found that among all considered systems, O-doped arsenene shows best HER activity followed by Nb-doped $ZrSe_2$.

CHAPTER 3
Effect of dopants on arsenene and zirconium chalcogenides based 2D catalysts towards hydrogen evolution reaction

References

[1] J.A. Turner, Energy View. **285**, 687 (1999).

[2] Rasul M. Clean Energy for Sustainable Development: Comparisons and Contrasts of New Approaches. Academic Press; (2017).

[3] M. Momirlan and T.N. Veziroglu, Int. J. Hydrogen Energy **30**, 795(2005).

[4] S.S. TONG, X.J. WANG, Q.C. LI, and X.J. HAN, Chinese J. Anal. Chem. **44**, 1447 (2016).

[5] S.H. Mir, S. Chakraborty, J. Wärnå, S. Narayan, P.C. Jha, P.K. Jha, and R. Ahuja, Catal. Sci. Technol. **7**, (2017).

[6] F. Pincella, K. Isozaki, and K. Miki, Light Sci. Appl. **3**, e133 (2014).

[7] J. Di, C. Yan, A.D. Handoko, Z.W. Seh, H. Li, and Z. Liu, Mater. Today **21**, 749(2018).

[8] J. Ran, J. Zhang, J. Yu, M. Jaroniec, and S.Z. Qiao, Chem. Soc. Rev. **43**, 7787(2014).

[9] R. Li and C. Li, Photocatalytic Water Splitting on Semiconductor-Based Photocatalysts, 1ed. In Advances in catalysis, **60**, 1-57. Academic Press, (2017).

[10] A. Eftekhari, Int. J. Hydrogen Energy **42**, 11053 (2017).

[11] J.E. Trancik, Nature **507**, 300 (2014).

[12] T. Shinagawa, A.T. Garcia-Esparza, and K. Takanabe, Sci. Rep. **5**, 13801(2015).

[13] J. Lee, S. Kang, K. Yim, K.Y. Kim, H.W. Jang, Y. Kang, and S. Han, J. Phys. Chem. Lett. **9**, 2049 (2018).

[14] N. Cheng, S. Stambula, D. Wang, M.N. Banis, J. Liu, A. Riese, B. Xiao, R. Li, T.K. Sham, L.M. Liu, G.A. Botton, and X. Sun, Nat. Commun., 13638 (2016).

[15] H. Yin, S. Zhao, K. Zhao, A. Muqsit, H. Tang, L. Chang, H. Zhao, Y. Gao, and Z. Tang, Nat. Commun. **6**, 6430 (2015).

[16] S. Cao, Y. Chen, C.-J. Wang, P. He, and W.-F. Fu, Chem. Commun. **50**, 10427 (2014).

[17] F. Safizadeh, E. Ghali, and G. Houlachi, Int. J. Hydrogen Energy **40**, 256 (2015).

[18] X. Chen, K. Yu, Y. Shen, Y. Feng, Z. Zhu, S. Min, J. Qin, W. Hai, Y. Lei, J. Hou, F. Wang, S. Kumar, N.L. Reddy, A. Kumar, M.V. Shankar, V. Krishnan, A. V. Dolganov, O. V. Tarasova, A.Y. Ivleva, O.Y. Chernyaeva, K.A. Grigoryan, V.S. Ganz, C. Torres, B. Moreno, E. Chinarro, C. de Fraga Malfatti, Q.F. Wang, R.P. Yanzhang, X.N. Ren, H. Zhu, M. Zhang, and M.L. Du, Int. J. Hydrogen Energy **42**, 20410 (2017).

[19] L. Yang, W. Zhou, D. Hou, K. Zhou, G. Li, Z. Tang, L. Li, and S. Chen, Nanoscale **7**, 5203 (2015).

[20] H. Li, M. Du, M.J. Mleczko, A.L. Koh, Y. Nishi, E. Pop, A.J. Bard, and X. Zheng, J. Am. Chem. Soc. **138**, 5123 (2016).

[21] S.H. Mir, S. Chakraborty, P.C. Jha, J. Wärnå, H. Soni, P.K. Jha, and R. Ahuja, Appl. Phys. Lett. **109**, (2016).

[22] S.H. Mir, S. Chakraborty, J. Wärnå, S. Narayan, P.C. Jha, P.K. Jha, and R. Ahuja, Catal. Sci. Technol. **7**, 687 (2017).

[23] G. Long, K. Wan, M. Liu, Z. Liang, J. Piao, and P. Tsiakaras, J. Catal. **348**, 151 (2017).

[24] N.N. Som, V. Mankad, and P.K. Jha, Int. J. Hydrogen Energy **43**, 21634 (2018).

[25] Y. Qu, H. Pan, C.T. Kwok, and Z. Wang, Nanoscale Res. Lett. **10**, 1 (2015).

[26] B. Feng, J. Zhang, Q. Zhong, W. Li, S. Li, H. Li, P. Cheng, S. Meng, L. Chen, and K. Wu, Nat. Chem. **8**, 563 (2016).

[27] X. Chen, K. Yu, Y. Shen, Y. Feng, and Z. Zhu, ACS Appl. Mater. Interfaces **9**, 42139 (2017).

[28] S. Min, J. Qin, W. Hai, Y. Lei, J. Hou, and F. Wang, Int. J. Hydrogen Energy **48**, 42139 (2018).

[29] J. Seok, J.H. Lee, S. Cho, B. Ji, H.W. Kim, M. Kwon, D. Kim, Y.M. Kim, S.H. Oh, S.W. Kim, Y.H. Lee, Y.W. Son, and H. Yang, 2D Mater. **4**, 025061 (2017).

[30] B.A. Bhanvase, T.P. Shende, and S.H. Sonawane, Environ. Technol. Rev. **6**, 1 (2017).

[31] Y. Chen, K. Yang, B. Jiang, J. Li, M. Zeng, and L. Fu, J. Mater. Chem. A **5**, 8187 (2017).

[32] J. Zhang, S. Jia, I. Kholmanov, L. Dong, D. Er, W. Chen, H. Guo, Z. Jin, V.B. Shenoy, L. Shi, and J. Lou, ACS Nano **11**, 8192 (2017).

[33] D. Er, H. Ye, N.C. Frey, H. Kumar, J. Lou, and V.B. Shenoy, Nano Lett. **18**, 3943 (2018).

[34] W. Shi and Z. Wang, J. Phys. Condens. Matter **30**, 21 (2018).

[35] S. Li, C. Wang, and H. Qiu, Int. J. Hydrogen Energy **40**, 15503 (2015).

[36] J.P. Perdew and K. Burke, Phys. Rev. B - Condens. Matter Mater. Phys. **54**, 16533 (1996).

[37] J. Perdew, K. Burke, and M. Ernzerhof, Phys. Rev. Lett. **77**, 3865 (1996).

[38] P. Giannozzi, S. Baroni, N. Bonini, M. Calandra, R. Car, C. Cavazzoni, D. Ceresoli, G.L. Chiarotti, M. Cococcioni, I. Dabo, A. Dal Corso, S. De Gironcoli, S. Fabris, G. Fratesi, R. Gebauer, U. Gerstmann, C. Gougoussis, A. Kokalj, M. Lazzeri, L. Martin-Samos, N. Marzari, F. Mauri, R. Mazzarello, S. Paolini, A. Pasquarello, L. Paulatto, C. Sbraccia, S. Scandolo, G. Sclauzero, A.P. Seitsonen, A. Smogunov, P. Umari, and R.M. Wentzcovitch, J. Phys. Condens. Matter **21**, (2009).

[39] S. Grimme, J. Antony, S. Ehrlich, and H. Krieg, J. Chem. Phys. **132**, 15104 (2010).

[40] H.J. Monkhorst and J.D. Pack, Phys. Rev. B - Condens. Matter Mater. Phys. **13**, 5188 (1976).

[41] J. Greeley, T.F. Jaramillo, J. Bonde, I. Chorkendorff, and J.K. Nørskov, Nat. Mater. **5**, 909 (2006).

[42] Y. Qu, H. Pan, C.T. Kwok, and Z. Wang, Nanoscale Res. Lett. **10**, 1 (2015).

[43] C.J. Rupp, S. Chakraborty, J. Anversa, R.J. Baierle, and R. Ahuja, ACS Appl. Mater. Interfaces **8**, 1536 (2016).

[44] P. Liao, J.A. Keith, and E.A. Carter, J. Am. Chem. Soc. **134**, 13296 (2012).

[45] A.R. Zeradjanin, A. Vimalanandan, G. Polymeros, A.A. Topalov, K.J.J. Mayrhofer, and M. Rohwerder, Phys. Chem. Chem. Phys. **19**, 17019 (2017).

[46] I. Union, O.F. Pure, and A. Chemistry **209**, 955 (1999).

[47] M.Y. Liu, Y. Huang, Q.Y. Chen, C. Cao, and Y. He, Sci. Rep. **6**, 29114 (2016).

[48] Z. Li, W. Xu, Y. Yu, H. Du, K. Zhen, J. Wang, L. Luo, H. Qiu, and X. Yang, J. Mater. Chem. C **4**, 362 (2016).

[49] J.K. Nørskov, T. Bligaard, J. Rossmeisl, and C.H. Christensen, Nat. Chem. **1**, 37 (2009).

[50] Y. Qu, H. Pan, and C.T. Kwok, Sci. Rep. **6**, 1 (2016).

[51] H. Jiang, J. Chem. Phys. **134**, 204705 (2011).

[52] H.B. Michaelson, J. Appl. Phys. **48**, 4729 (1977).

[53] M.R. Gao, M.K.Y. Chan, and Y. Sun, Nat. Commun. **6**, 1 (2015).

[54] T.F. Jaramillo, K.P. Jørgensen, J. Bonde, J.H. Nielsen, S. Horch, and I. Chorkendorff, Science **317**, 100 (2007).

[55] P. Liu, J. Zhu, J. Zhang, P. Xi, K. Tao, D. Gao, and D. Xue, ACS Energy Lett. **2**, 745 (2017).

[56] J. Wang, J. Liu, B. Zhang, X. Ji, K. Xu, C. Chen, L. Miao, and J. Jiang, Phys. Chem. Chem. Phys. **19**, 10125 (2017).